STUDY OF OXYGEN EVOLUTION REACTION ON IRON GROUP-BASED ELECTRODEPOSITED MULTICOMPONENT CATALYSTS IN ALKALINE MEDIA. PART II: SURFACE INVESTIGATIONS AND CORROSION DURABILITY

Vasil Bachvarov[1], Marina Arnaudova[1], Elefteria Lefterova[2], Rashko Rashkov[1]

[1]*Institute of Physical Chemistry, Bulgarian Academy of Sciences*
11 Acad. G. Bonchev Str., 1113 Sofia, Bulgaria
[2]*Institute of Electrochemistry and Energy Systems*
Bulgarian Academy of Sciences, 10 Acad. G. Bonchev Str.
1113 Sofia, Bulgaria
E-mail address: rasho@ipc.bas.bg

Received 18 March 2022
Accepted 05 August 2022

ABSTRACT

This paper looks into the electrochemically active surface area (ECSA) of $Mo_{34}Ni_{26}Co_{25}Fe_{15}$, $Ni_{32}W_{31}Co_{19}Fe_{18}$, $Mo_{35}Co_{29}Ni_{21}Fe_{15}$, $Co_{32}Fe_{30}W_{20}Ni_{18}$ $Ni_{56}Fe_{21}Co_{13}P_{10}$. The results show an inverse relationship between the active surface and the alloy overpotential for oxygen evolution reaction (OER). XPS is applied for Ni, Co, Fe, Mo, W and P valence state determination on quaternary systems. The better electrocatalytic activity of $Mo_{35}Co_{29}Ni_{21}Fe_{15}$ and $Co_{32}Fe_{30}W_{20}Ni_{18}$ alloys compared to $Mo_{34}Ni_{26}Co_{25}Fe_{15}$ and $Ni_{32}W_{31}Co_{19}Fe_{18}$ could be attributed to the interaction between individual elements, especially Co and Fe, and to the quantitative ratio between them in the general electronic configuration. The best catalytic activity of $Ni_{56}Fe_{21}Co_{13}P_{10}$ alloy for OER is considered to be associated with phosphate presence on the surface. In addition, the latter alloy shows great corrosion and mechanical durability. The electrocatalytic activity of $Ni_{56}Fe_{21}Co_{13}P_{10}$ for OER remains unchanged after 105 hours of anodic polarization at i = 100 mA cm^{-2}.

Keywords: oxygen evolution reaction, electrocatalytic activity, XPS, corrosion resistance, NiFeCoP.

INTRODUCTION

Alloying two or more metals affects the catalytic properties of materials because the electronic structure, especially in the d-orbitals, changes. Chemical elements located at the left- hand side of the transition series have vacant d-orbital (hypo-d-electron metals as Mn, Zr, Mo, W). Those at the right-hand side have filled inner twin d-orbitals (hyper-d-electron metals as Ni, Co, Fe). A combination of such elements results in an electron interaction and modification of the surface (binding) energy of the intermetallic compounds obtained. This interaction increases stability of the catalyst [1, 2].

An important requirement for a good catalytic activity is a highly developed surface, which grants a larger number of active sites. Material amorphization is one way of meeting this requirement. Amorphous materials have a high concentration of unsaturated sites at the surface and enhance surface reaction rate because they improve adsorption as compared to the corresponding crystalline catalysts [3]. It has been established that phosphate formation in an amorphous NiFeP alloy [4] generates active sites for OER while Fe improves additionally the intrinsic activity. A hierarchical flower-like structure of Ni-Fe-Co-based mixed metal/metal-oxides nanoparticles encapsulated in ultrathin carbon nanosheets (via a simple pyrolysis process) is responsible for the excellent OER activity. It is a consequence of the enhanced surface area and improved intrinsic catalytic performance [5]. Surface phosphides [6, 7] and phosphates [8] formed on iron and cobalt-nickel matrices demonstrate excellent catalytic properties for OER, thus offering a possibility of their commercial application in water splitting electrodes which do not contain precious metals.

OER activity of Ni + Mo and Ni + Mo + Si coatings has been established to be much higher than that of the pure nickel and is considered to be associated mainly

with active surface enlargement [10]. Iron doping of $NiMoO_4$ matrix enhances the catalytic activity for OER which is accredited to the higher number of unpaired *d*-electrons in the oxides [10]. With a suitable transition metal added to modulate the 3d-transition in metal oxyhydroxides, additional opportunities open up for an improved OER. Tungsten has been confirmed as such a modulator and at its highest oxidation state, it acts as a structural multifunctional coordinator [11]. A gelled-FeCoW obtained by the sol-gel method on gilded nickel foam shows low overpotential and high stability for OER.

This suggests that it is not only the developed surface but also the electronic interaction between the individual components playing a crucial role in elevating electrocatalytic activity.

In our previous work [12], we have shown that 4-component alloys based on Ni-Fe-Co doped with Mo, W and P have better catalytic properties than pure nickel and its binary and ternary alloys. OER catalytic activity of these systems line up in the following sequence: $Mo_{34}Ni_{26}Co_{25}Fe_{15} < Ni_{32}W_{31}Co_{19}Fe_{18} < Mo_{35}Co_{29}Ni_{21}Fe_{15} < Co_{32}Fe_{30}W_{20}Ni_{18} < Ni_{56}Fe_{21}Co_{13}P_{10}$.

This paper focuses on identifying the predominant factor in achieving a better catalytic activity of the systems studied - whether it is the surface or the interaction between alloy components. To avoid substrate surface influence, a smooth copper plate was used for electrodeposition.

EXPERIMENTAL

Quaternary alloys were electrodeposited under conditions detailed in our previous work [12]. Fischerscope® X-RAY system (X-ray fluorescence analysis; XRF) was used to determine change in coating composition and thickness. Element valence states were determined by X-ray photoelectron spectroscopy (XPS). Measurements were carried out on AXIS Supra electron spectrometer (Kratos Analytical Ltd.) using monochromatic AlKα and MgKα radiation with photon energy of 1486.6 eV and 1253.6 eV, respectively. Energy calibration was done by normalizing the C1s line of adsorbed adventitious hydrocarbons to 284.6 eV. Binding energies (BE) were determined with an accuracy of ± 0.1 eV. A commercial data-processing software (Kratos Analytical Ltd.) was applied for peak deconvolution.

A special procedure was applied to observe the change in element valence state at the surface after oxygen generation process - "after OER". The procedure involved two steps: first - a 15 min anode polarization of the electrodes at 100 mA cm^{-2} to boost formation of metal oxides and/or oxyhydroxides on alloy surface and second - determination of OER catalytic activity of systems studied in [12] while ensuring reproducible results (with Linear Sweep Voltammetry (LSV) method at a scan rate of 0.1 mV s^{-1}). Polarization curves were applied to measure OER activity after a long-term stability test using Potensiostat/Galvanostat Gamry (version 6.25) equipment.

RESULTS AND DISCUSSION

ECSA measurements

SEM observations have not provided a clear answer whether the surface is responsible for the difference in electrocatalytic behaviour observed between quaternary alloys [12]. To explore deeper the relationship between surface and catalytic properties, capacitive measurements were performed to determine the electrochemically active surface area (ECSA). ECSA was determined by the double layer capacity (C_{dl}). Capacitive curves in the region of approximately ± 100 mV, relative to open-circuit potential (OCP) where no Faraday reaction takes place, service to define ΔI at different scan rates [13, 14].

$$\Delta I = (|I_a| - |I_c|) / 2 , \quad (1)$$

where Ia and Ic are the anodic and cathodic current, respectively, at the same potential at which the condition Ia ≈ Ic is fulfilled.

ΔI dependence on scan rate is presented in Fig. 1. The slope corresponded to C_{dl}, proportional to ECSA, i.e. a higher value for C_{dl} corresponded to a more developed ECSA and a larger number of active sites. ECSA was calculated from equation 2

$$ECSA = C_{dl}/C_s, \quad (2)$$

where C_s is the capacity of smooth metallic electrode = 20 μF cm^{-2} [15, 16]. A developed surface implied better catalytic behavior of the material. Fig. 1 and Table 1 data comparison showed that the highest value of C_{dl} belonged to $Mo_{34}Ni_{26}Co_{25}Fe_{15}$ alloy, i.e. the largest

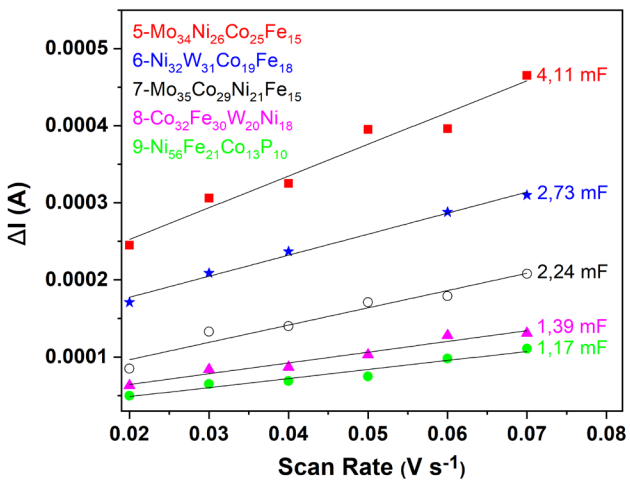

Fig. 1. Capacitive current *vs* scan rate for determining ECSA of the quaternary alloys.

Table 1. The calculated value of ECSA and corresponding overpotential (η) for i=100 mA cm^{-2} presented in [12].

Samples	C_{dl}, mF	ECSA cm^2	$\eta_{i=100}$ V
$5\text{-}Mo_{34}Ni_{26}Co_{25}Fe_{15}$	4.11	205.5	0.469
$6\text{-}Ni_{32}W_{31}Co_{19}Fe_{18}$	2.73	136.5	0.432
$7\text{-}Mo_{35}Co_{29}Ni_{21}Fe_{15}$	2.24	112.0	0.416
$8\text{-}Co_{32}Fe_{30}W_{20}Ni_{18}$	1.39	69.5	0.411
$9\text{-}Ni_{56}Fe_{21}Co_{13}P_{10}$	1.17	58.5	0.393

surface area though the highest overpotential (η), as presented in [12]. In contrast, $Ni_{56}Fe_{21}Co_{13}P_{10}$ system demonstrated the lowest overpotential, meaning the best catalytic activity appeared at the least developed surface (lowest C_{dl} value). The other systems exhibited similar inverse correlation between overpotential and ECSA, i.e. the real surface (RS) decreased in the following order: $RS_{Mo34Ni26Co25Fe15} > RS_{Ni32W31Co19Fe18} > RS_{Mo35Co29Ni21Fe15} > RS_{Co32Fe30W20Ni18} > RS_{Ni56Fe21Co13P10}$. As for the catalytic activity, it increased [12] as follows: $Mo_{34}Ni_{26}Co_{25}Fe_{15} < Ni_{32}W_{31}Co_{19}Fe_{18} < Mo_{35}Co_{29}Ni_{21}Fe_{15} < Co_{32}Fe_{30}W_{20}Ni_{18} < Ni_{56}Fe_{21}Co_{13}P_{10}$. It was made apparent that for the catalytic activity of the systems studied, the determining factor was not the surface, but rather the interaction between alloy components and the products formed as a result of OER.

XPS characterization

XPS was applied to determine Ni, Co, Mo, W and P valence state in NiCoFeMo, NiCoFeW and NiFeCoP systems, respectively. Figs. 2 - 4 depict XPS spectra of fresh electrodeposited alloys as well as of alloys subjected to the experimental procedure described above. Three main peaks in $Ni2p_{3/2}$ region were observed for the fresh samples (Fig. 2(a) and Fig. 3(a)). Binding energies (BE) for $Ni2p_{3/2}$ were in the region of ~852.3 eV due to Ni^0 and/or NiM alloy (M = Co, Fe, Mo, W). Binding energies in the range of 854 - 857 eV and satellite peaks above 858 eV were considered associated with Ni^{II}/Ni^{III} in NiO, $Ni(OH)_2$, NiOOH, and mixed oxides/hydroxide (Fig. 5(a) and 6(a)). The peak at ~856 eV together with the satellite peak strongly increased at the expense of the one at 852.3 eV, which was due to Ni^0oxidation after oxygen evolution. Although Ni^{II} and Ni^{III} were difficult to distinguish, the deconvoluted spectra corresponded more to Ni^{II} [17]. A possible explanation of Ni^{II} predomination after OER could be that Co, Mo or W suppressed electrochemical oxidation of $Ni(OH)_2$ to NiOOH, just like it has been established for Fe [18]. In $Co2p_{3/2}$ region, peaks at 778 eV, 779.8 eV and 781 eV together with a satellite one at 786.7 eV (Fig. 2(b) and 3(b)) referred to Co^0, Co^{III} and Co^{II}, respectively [17, 19]. In fresh NiCoFeMo samples, Co^{II} and Co^{III} coexisted on the surface, but Co^{II} dominated in tungsten containing alloys. After OER, Co^{III} species dominated in NiCoFeMo samples, while both Co^{II} and Co^{III} were present in NiCoFeW samples. Iron was present in Fe^{II}/Fe^{III} valence states in all samples tested (Fig. 4(a)).

XPS spectrum of fresh sample Mo3d region (Fig. 2(c)) could be deconvoluted with 4 doublets at 227.8 eV, 229.7 eV, 231.1 eV and 232.2 eV corresponding to Mo^0, Mo^{IV}, Mo^V and Mo^{VI} valence states [20]. After OER, the highest oxidation level of molybdenum Mo^{VI} was reached. The higher electrocatalytic activity of $Mo_{35}Co_{29}Ni_{21}Fe_{15}$ compared with $Mo_{34}Ni_{26}Co_{25}Fe_{15}$ could be attributed to the relatively larger cobalt quantity leading to formation of a higher active site number (Co^{III} - CoOOH) for oxygen generation. Xiaobo et al. have established that increase in Co^{III} surface content improves the catalytic activity for OER [21].

The W4f spectral region (Fig. 3(c)) of fresh catalysts showed 2 states of tungsten, respectively, W^0 at 31.3 eV and W^{VI} at 35.6 eV. After OER, dominant was W^{VI} with a small W^{IV} amount in the $Ni_{32}W_{31}Co_{19}Fe_{18}$ alloy and

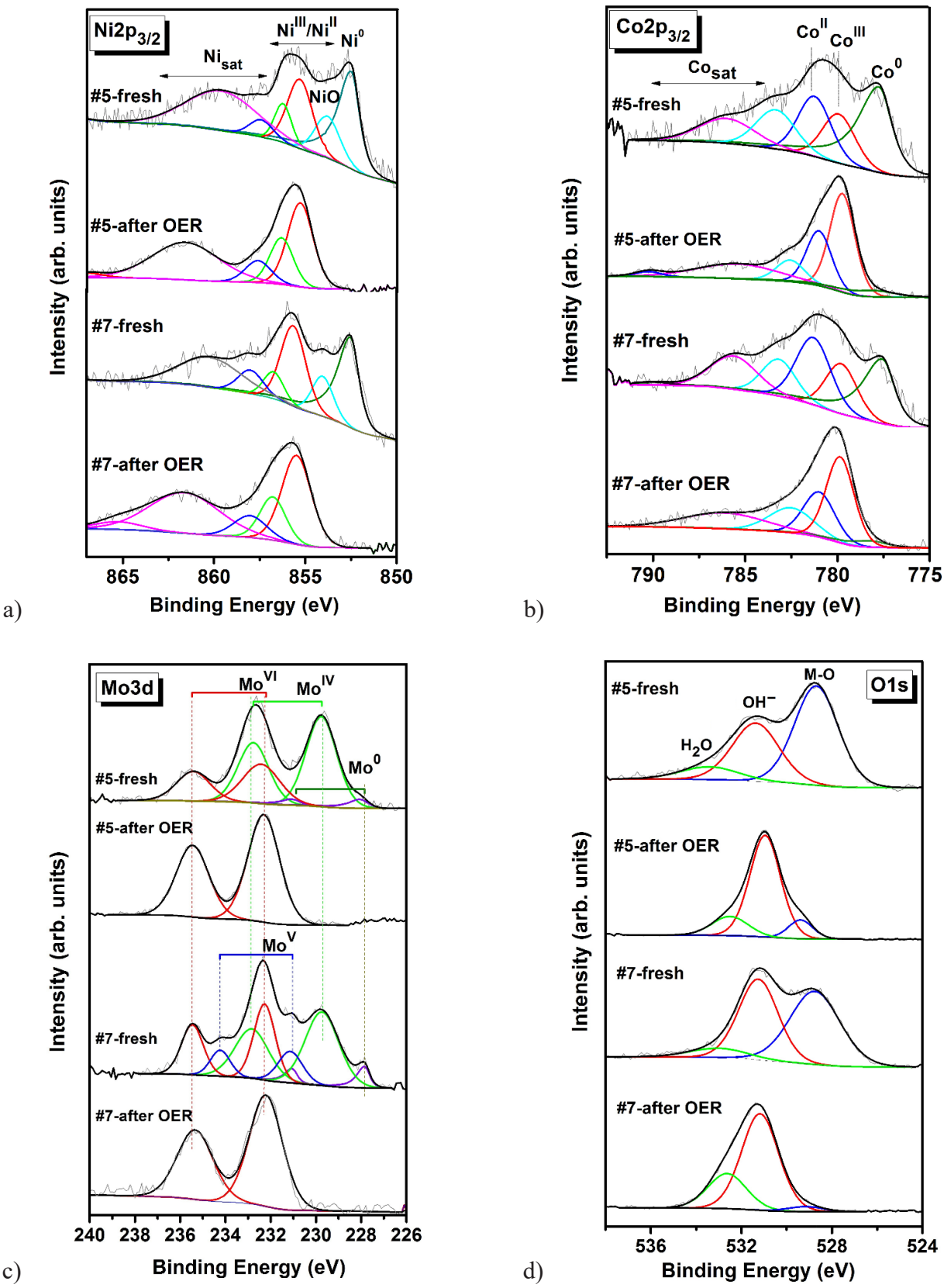

Fig. 2. XPS spectra of the catalysts #5 - $Mo_{34}Ni_{26}Co_{25}Fe_{15}$ and #7 - $Mo_{35}Co_{29}Ni_{21}Fe_{15}$ fresh and after OER (a) Ni $2p_{3/2}$, (b) $Co2p_{3/2}$, (c) Mo3d, (d) O1s.

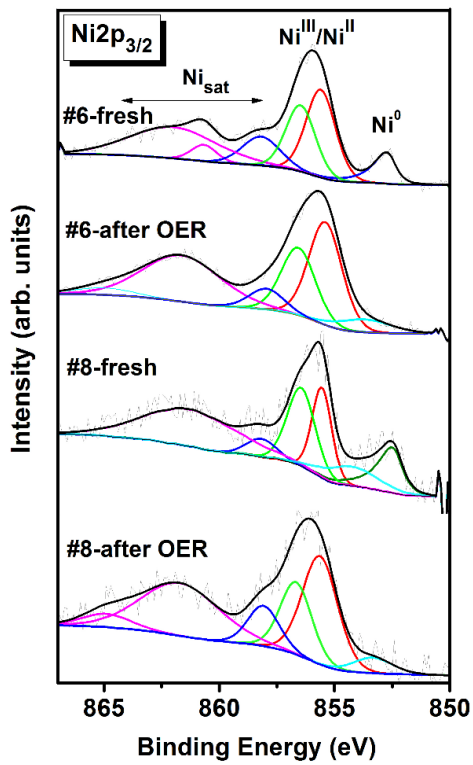

a)

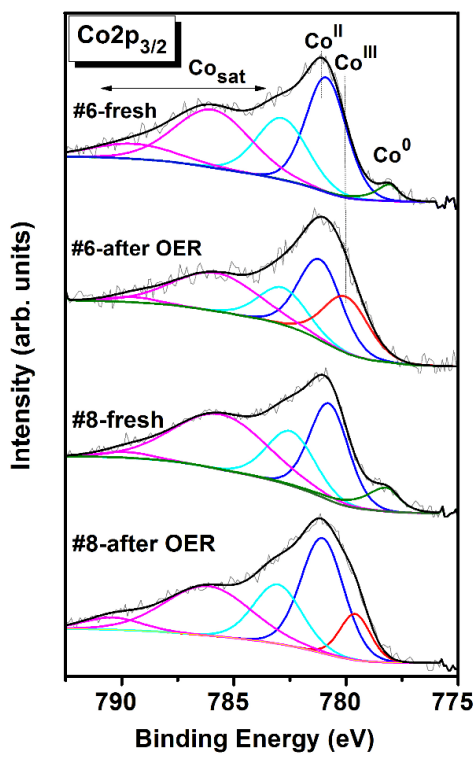

b)

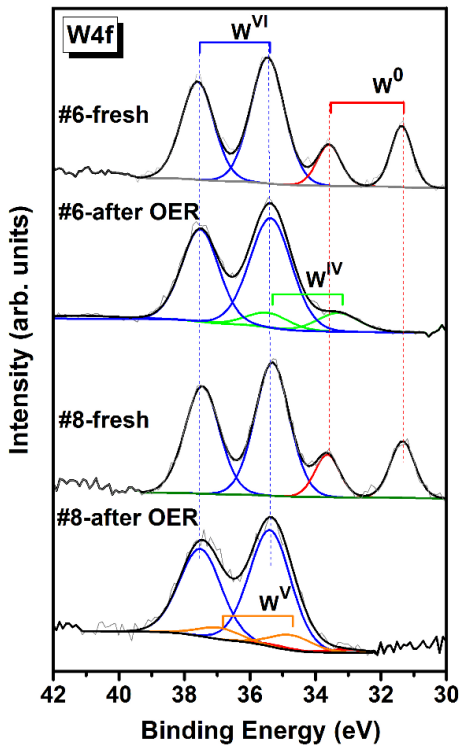

c)

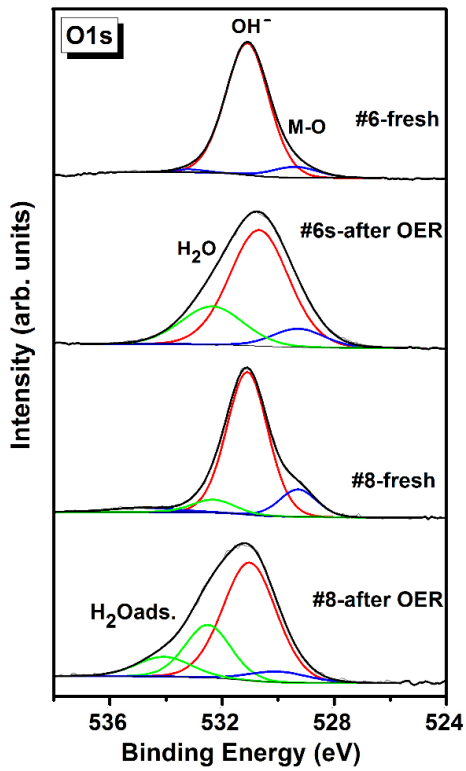

d)

Fig. 3. XPS spectra of the catalysts #6 - $Ni_{32}W_{31}Co_{19}Fe_{18}$ and #8 - $Co_{32}Fe_{30}W_{20}Ni_{18}$ fresh and after OER (a) Ni $2p_{3/2}$, (b) $Co2p_{3/2}$, (c) W4f, (d) O1s.

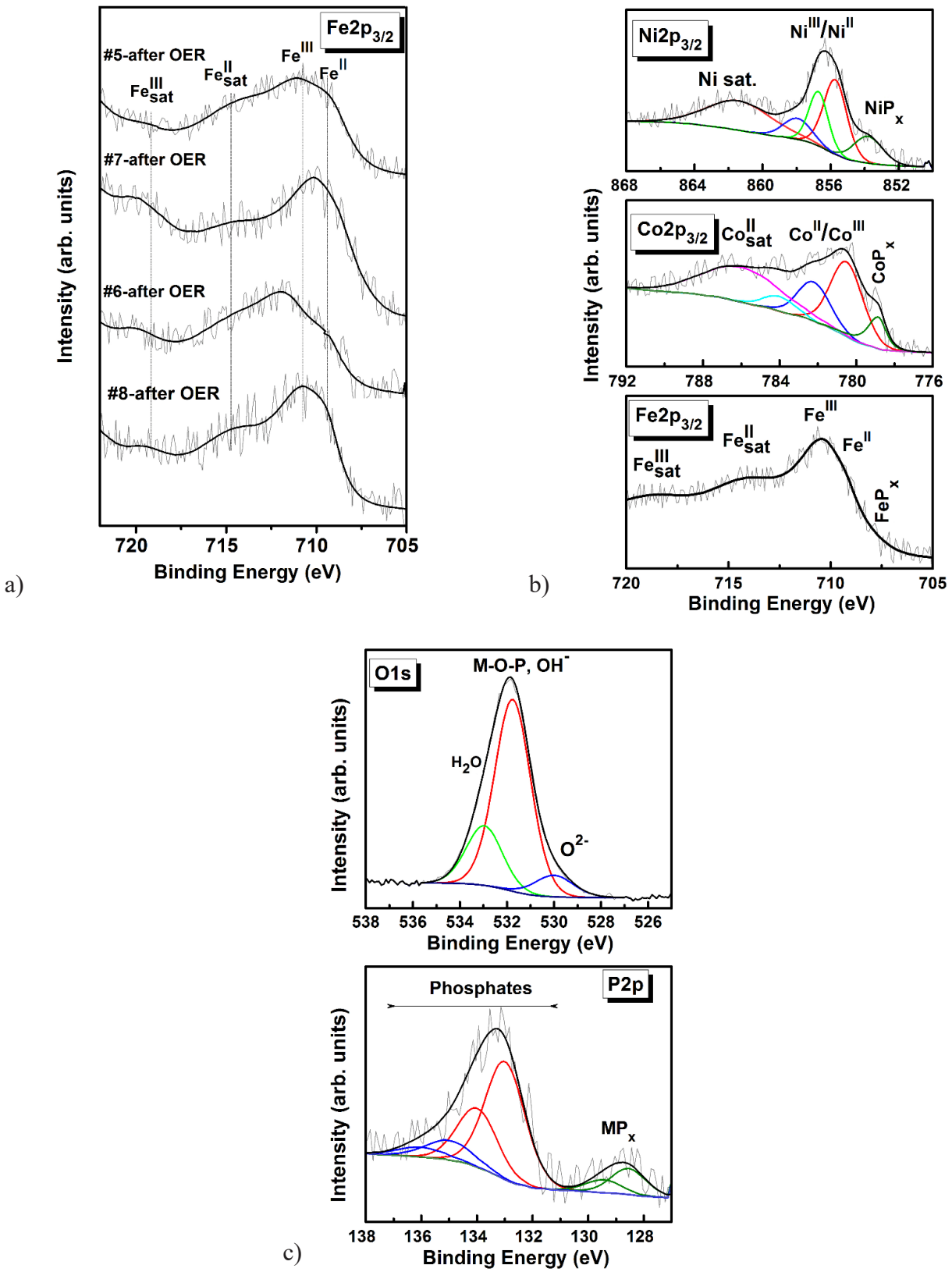

Fig. 4. XPS spectra of (a) $Fe2p_{3/2}$ of the catalysts #5 - $Mo_{34}Ni_{26}Co_{25}Fe_{15}$, #7- $Mo_{35}Co_{29}Ni_{21}Fe_{15}$, #6 - $Ni_{32}W_{31}Co_{19}Fe_{18}$ and #8 - $Co_{32}Fe_{30}W_{20}Ni_{18}$ after OER, (b) Ni $2p_{3/2}$, $Co2p_{3/2}$ and $Fe2p_{3/2}$ of $Ni_{56}Fe_{21}Co_{13}P_{10}$ catalyst after OER, (c) O1s and $P2p_{3/2}$ of $Ni_{56}Fe_{21}Co_{13}P_{10}$ catalyst after OER.

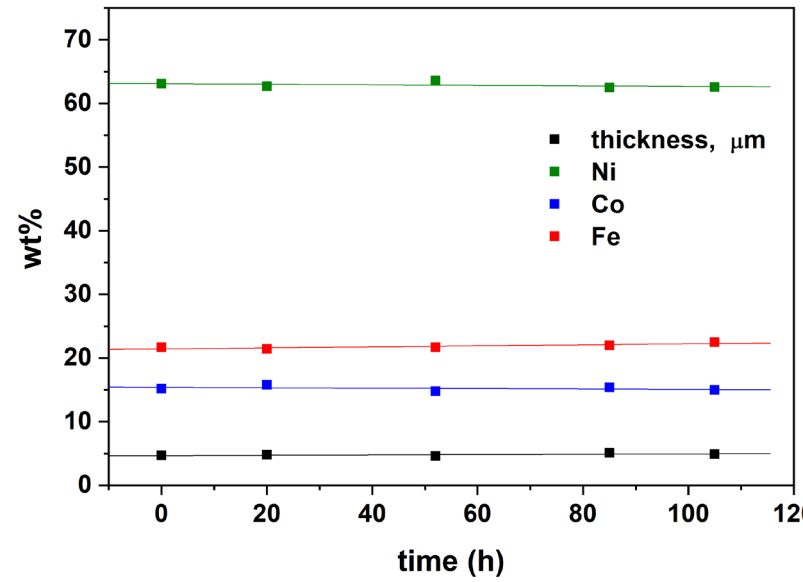

a)

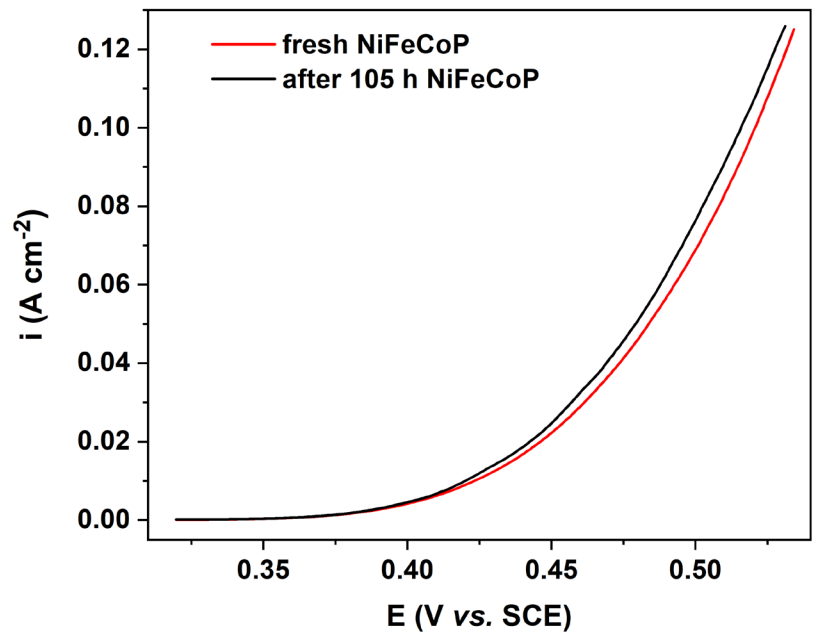

b)

Fig. 5. (a) Dependence of the weight percentage of components in the NiFeCoP alloy with time at anodic polarization (100 mA cm^{-2}), (b) polarizations curves of fresh and after the stability test NiFeCoP alloy.

W^V in $Co_{32}Fe_{30}W_{20}Ni_{18}$ [20]. The latter exhibited better electrocatalytic activity for OER. This could be justified mainly by the higher cobalt and iron content [10, 22].

It has been assumed that Mo^{6+} and W^{6+} species withdraw electrons of 3d metals and lead to redistribution of electron configuration [23]. In evidence to this assumption is their lower BE (by about 0.2 - 0.4 eV) compared to pure MO_3 oxides (BE_{MoO3} = 232.6 eV; BE_{WO3} = 35.6 eV).

High resolution O1s spectra are presented in Fig. 2(d) and 3(d). The two peaks centered at 529 - 530 eV and 531 - 532 eV were associated with M-O and M-O-H bonds, respectively. The presence of the first peak for the fresh samples was an indication for the MO_x species. It dominated on fresh NiCoFeMo samples and decreased sharply after OER. The second peak

was due to formation of $M(OH)_x$ on the fresh samples and dominated on NiCoFeW samples. This peak was the main component in the O1s spectra of all catalysts after OER. These results correlated with the rest XPS spectra and proved the formation of mixed hydroxides/oxyhydroxides $M^{hyper}M^{hypo}O_x(OH)_y$ (where M^{hyper} = S(Ni,Fe,Co) and M^{hypo} = W, Mo) during OER.

Analysis of Ni, Co and Fe 2p XPS peaks and satellite structure in Fig. 4(b) showed that after OER on $Ni_{56}Fe_{21}Co_{13}P_{10}$ alloy, the predominant valence state for nickel was Ni^{II}, for cobalt - it was Co^{II}, while for iron - it was Fe^{II} and Fe^{III}. As established previously [24], phosphorous doping occurs mainly via nickel and/or cobalt phosphides. The P2p spectral region of the oxidized sample (Fig. 4(c)) showed that mainly phosphates and a bit phosphide were present on the surface. The position of the strongest P2p doublet (at ~133 eV) corresponded to pyrophosphate $(P_2O_7)^{4-}$ units in $M_2P_2O_7$ (M = Ni, Co) and therefore, Ni and Co were in second valence in this compound. Evidently, during the process of anodic polarization, phosphides were oxidized to phosphates. Formation of a phosphate in the amorphous NiFeP alloy generated active sites for OER [4], such sites being responsible for the better electrocatalytic activity of $Ni_{56}Fe_{21}Co_{13}P_{10}$ alloy compared to the other systems studied.

System complexity suggested that the interaction between the individual elements was of importance as well as the impact of their quantitative ratio on the general electronic configuration. On the one hand, there was electronic interaction between hyper- (Fe, Ni, Co) and hypo-d-elements as Mo, W. On the other hand, the different degree of oxidation was directly related to the electronic conductivity [25]. The role of iron should be emphasized here since its inclusion boosted catalytic activity of oxide [18, 26] and hydroxide systems [25, 27]. The presence of phosphates also contributed to a better catalytic activity.

Long term stability test

A basic requirement for the practical application of OER catalysts refers to their stability during prolonged operation at high anodic current densities. A long-term stability test was performed in 6M KOH at 100 mA cm^{-2} anodic polarization to check the corrosion and mechanical resistance of the quaternary alloys. During the anodic polarization, coatings containing Mo and W were mechanically destroyed from the copper substrate after 30 - 40 hours. Probable reasons for such a behavior were considered to be high internal stresses in the alloys and poor adhesion to the substrate. Only $Ni_{56}Fe_{21}Co_{13}P_{10}$ alloy, polarized for 105 hours at an anodic current density of 100 mA cm^{-2}, remained stable throughout the process. Coating composition and thickness were monitored by X-ray fluorescence analysis. At certain intervals, the sample was analyzed at 5 different points and at certain intervals to detect component composition and thickness values, the latter being averaged. The built-in millimeter scale of the device allowed for measurements at the same points for each time-interval. Fig. 5(a) illustrates the dependence of each component percentage content and layer thickness on anodic polarization time. The results showed insignificant deviations in the composition and thickness of the catalytic layer studied. $Ni_{56}Fe_{21}Co_{13}P_{10}$ alloy exhibited excellent corrosion and mechanical resistance in 6M KOH.

The long-term stability test showed a persisting OER electrocatalytic activity of the alloy. No significant differences in the polarization curves (Fig. 5(b)) of the $Ni_{56}Fe_{21}Co_{13}P_{10}$ electrode before and after the test (105 hours) were observed. These results demonstrated that the system studied possessed excellent catalytic activity, and corrosion and mechanical stability in the course of a prolonged oxygen generation. This, in turn, substantiates alloy system application in practice as an anode material in water splitting.

CONCLUSIONS

High OER electrocatalytic activity of the alloy could be explained by formation of mixed hydroxides/oxyhydroxides $M^{hyper}M^{hypo}O_x(OH)_y$ (M^{hyper} = S (Ni, Fe, Co) and M^{hypo} = W, Mo). These ensure a synergy between Fe, Co and Ni hyper-d elements, on the one hand, and on the other, a hypo-hyper-d interaction between hypo-d and hyper-d elements. The presence of Mo and W highest valence leads to an electron density redistribution due to the attraction of electrons from the hyper d-elements. The general electronic configuration in the multicomponent systems depends on the quantitative ratio and interaction between the individual elements. In this sense, the better catalytic properties of $Mo_{35}Co_{29}Ni_{21}Fe_{15}$ and $Co_{32}Fe_{30}W_{20}Ni_{18}$ alloys compared

to $Mo_{34}Ni_{26}Co_{25}Fe_{15}$ and $Ni_{32}W_{31}Co_{19}Fe_{18}$ are explained by the higher Co content and the specific role of Fe. This is why the surface is not a determinant of catalytic activity, as indicated by ECSA calculation for quaternary alloys. The results indicate an inverse relationship - at a more developed surface, higher overpotentials for OER mean worse OER catalytic activity. In addition, the different degree of oxidation facilitates charge transfer and increases conductivity. Phosphate presence on the $Ni_{56}Fe_{21}Co_{13}P_{10}$ alloy surface is the reason for the best OER catalytic activity. Furthermore, this alloy shows great corrosion and mechanical durability, which points towards alloy possible application in practice.

Acknowledgements

This work was supported by the Bulgarian Ministry of Education and Science under the National Research Programme "Low Carbon Energy for the Transport and Households" (E+), grant agreement D01-214/2018.

REFERENCES

1. J.M. Jakšić, M.V. Vojnović, N.V. Krstajić, Kinetic analysis of hydrogen evolution at Ni-Mo alloy electrodes, Electrochem. Acta, 45, 2000, 4151-4158. https://doi.org/10.1016/S0013-4686(00)00549-1
2. M.M. Jaksic, Hypo-hyper-d-electronic interactive nature of interionic synergism in catalysis for hydrogen reaction, Int. J. Hyd. Energy, 26, 2001, 559-578. https://doi.org/10.1016/S0360-3199(00)00120-8
3. H. Liang, A.N. Gandi, Ch. Xia, M.N. Hedhili, D.H. Anjum, U. Schwingenschlögl, H.N. Alshareef, Amorphous NiFe-OH/NiFeP Electrocatalyst fabricated at low temperature for water oxidation applications, ACS Energy Lett., 2, 2017, 1035-1042. https://doi.org/10.1021/acsenergylett.7b00206
4. F. Hu, Sh. Zhu, Sh. Chen, Y. Li, L. Ma, T. Wu, Y. Zhang, Ch. Wang, C. Liu, X.Yang, L. Song, X. Yang, Y. Xiong, Amorphous Metallic NiFeP: A Conductive bulk material achieving high activity for oxygen evolution reaction in both alkaline and acidic media, Adv. Mater., 29, 2017, 1-9. https://doi.org/10.1002/adma.201606570
5. W. Yaseen, N. Ullah, M. Xie, B.A. Yusuf, Y. Xu, C. Tong, J. Xie, Ni-Fe-Co based mixed metal/metal-oxides nanoparticles encapsulated in ultrathin carbon nanosheets: A bifunctional electrocatalyst for overall water splitting, Surf. Interfaces, 26, 2021, 101361. https://doi.org/10.1016/j.surfin.2021.101361
6. Y. Wang, B. Ma, Y. Chen, Iron phosphides supported on three-dimensional iron foam as an efficient electrocatalyst for water splitting reactions, J. Mater. Sci., 54, 2019, 14872-14883. https://doi.org/10.1007/s10853-019-03985-9
7. Y. Pang, W. Xu, S. Zhu, Z. Cui, Y. Liang, Z. Li, S. Wu, C. Chang, S. Luo, Self-supporting amorphous nanoporous NiFeCoP electrocatalyst for efficient overall water splitting, J. Mater. Sci. Technol., 82, 2021, 96-104. https://doi.org/10.1016/j.jmst.2020.11.020
8. J. Li, W. Xu, D. Zhou, J. Luo, D. Zhang, P. Xu, L. Wei, D. Yuan, Synthesis of 3D flower-like cobalt nickel phosphate grown on Ni foam as an excellent electrocatalyst for the oxygen evolution reaction, J. Mater., Sci. 53, 2018, 2077-2086. https://doi.org/10.1007/s10853-017-1631-3
9. J. Kubisztal, A. Budniok, Study of the oxygen evolution reaction on nickel-based composite coatings in alkaline media, Int. J. Hydrogen Energy 33, 17, 2008, 4488-4494. https://doi.org/10.1016/j.ijhydene.2008.06.023
10. M. Kumar, R. Awasthi, A.K. Pramanick, R.N. Singh, New ternary mixed oxides of Fe, Ni and Mo for enhanced oxygen evolution, Int. J. Hydrogen Energy, 36, 2011, 12698-12705. https://doi.org/10.1016/j.ijhydene.2011.07.029
11. B. Zhang, X. Zheng, O. Voznyy, R. Comin, M. Bajdich, M. García-Melchor at all, Homogeneously dispersed multimetal oxygen-evolving catalysts, Science, 352, 6283, 2016, 333-337. https://doi.org/10.1126/science.aaf1525
12. V. Bachvarov, M. Arnaudova, E. Lefterova, R. Rashkov, Study of the oxygen evolution reaction on iron group based electrodeposited multicomponent catalysts in alkaline media. Part I: The influence of composition, J. Chem. Technol. Met., 57, 5, 2022, 910-918.
13. Z. Ye, C. Qin, G. Ma, X. Peng, T. Li, D. Li, Z. Jin, Cobalt-iron oxide nanoarrays supported on carbon fibre paper with high stability for electrochemical oxygen evolution at large current densities, ACS

Appl. Mater. Interfaces, 10, 46, 2018, 39809-39818. https://doi.org/10.1021/acsami.8b15357

14. M. Xia, T. Lei, N. Lv, N. Li, Synthesis and electrocatalytic hydrogen evolution performance of Ni–Mo–Cu alloy coating electrode, Int. J. Hydrogen Energy, 39, 10, 2014, 4794-4802. https://doi.org/10.1016/j.ijhydene.2014.01.091
15. J. Liu, H. Watanabe, M. Fuji, M. Takahashi, Electrocatalytic evolution of hydrogen on porous alumina/gelcast-derived nano-carbon network composite electrode, Electrochem. Commun., 11, 1, 2009, 107-110. https://doi.org/10.1016/j.elecom.2008.10.032
16. R.K. Shervedani, A. Lasia, Studies of the hydrogen evolution reaction on Ni-P electrodes, J. Electrochem. Soc., 144, 2, 1997, 511-519. https://doi.org/10.1149/1.1838623
17. B.P. Payne, M.C. Biesinger, N.S. McIntyre, The study of polycrystalline nickel metal oxidation by water vapour, J. Electron. Spectrosc. Relat. Phenom., 175, 1-3, 2009, 55-65. https://doi.org/10.1016/j.elspec.2009.07.006
18. M.W. Louie, A.T. Bell, An investigation of thin-film Ni-Fe oxide catalysts for the electrochemical evolution of oxygen, J. Am. Chem. Soc., 135, 2013, 12329-12337. https://doi.org/10.1021/ja405351s
19. M.C. Biesinger, B.P. Payne, A.P. Grosvenor, L.W.M. Lau, A.R. Gerson, R.St.C. Smart, Resolving surface chemical states in XPS analysis of first row transition metals, oxides and hydroxides: Cr, Mn, Fe, Co and Ni, Appl. Surf. Sci., 257, 7, 2011, 2717-2730. https://doi.org/10.1016/j.apsusc.2010.10.051
20. S.F. Ho, S. Contarini, J.W. Rabalai, Ion-beam-induced chemical changes in the oxyanions (MO_y^{n-}) and oxides (MO_x) where M = Cr, Mo, W, V, Nb, and Ta, J. Phys. Chem., 91, 18, 1987, 4779-4788. https://doi.org/10.1021/j100302a027
21. H. Xiaobo, Y. Fengxiang, L. Guoru, A Co/metal-organic-framework bifunctional electrocatalyst: The effect of the surface cobalt oxidation state on oxygen evolution/reductionreactions in an alkaline electrolyte, Int. J. Hydrogen Energy, 40, 31, 2015, 9713-9722. https://doi.org/10.1016/j.ijhydene.2015.06.027
22. Z. Lu, W. Xu, W. Zhu, Q. Yang, X. Lei, J. Liu, Y. Li, X. Sun, X. Duan, Three-dimensional NiFe layered double hydroxide film for high-efficiency oxygen evolution reaction, Chem. Commun., 50, 2014, 6479-6482. https://doi.org/10.1039/C4CC01625D
23. P.F. Liu, S. Yang, L.R. Zheng, B. Zhang, H.G. Yang, Mo^{6+} activated multimetal oxygen-evolving catalysts, Chem. Sci., 8, 2017, 3484-3488. https://doi.org/10.1039/-C6SC04819F
24. V. Bachvarov, E. Lefterova, R. Rashkov, Electrodeposited NiFeCo and NiFeCoP alloy cathodes for hydrogen evolution reaction in alkaline medium, Int. J. Hydrogen Energy, 41, 30, 2016, 12762-12771. https://doi.org/10.1016/j.ijhydene.2016.05.164
25. M.B. Stevens, L.J. Enman, E.H. Korkus et all, Ternary Ni-Co-Fe oxyhydroxide oxygen evolution catalysts: Intrinsic activity trends, electrical conductivity, and electronic band structure, Nano Res., 12, 2019, 2288–2295. https://doi.org/10.1007/s12274-019-2391-y
26. Ch.-W. Chen, Ch.-Y. Chiang, Molybdenum-containing amorphous metal oxide catalysts for oxygen evolution reaction, Int. J. Hydrogen Energy, 42, 50, 2017, 29773-29780. https://doi.org/10.1016/j.ijhydene.2017.10.009
27. F. Song, M.M. Busch, B. Lassalle-Kaiser, C.S. Hsu, E. Petkucheva, M. Bensimon, H.M. Chen, C. Corminboeuf, X. Hu, An unconventional iron nickel catalyst for the oxygen evolution reaction, ACS Central Sci., 5, 3, 2019, 558-568. https://doi.org/10.1021/acscentsci.9b00053